Kilohertz-Frequency Rotation of Acoustically Levitated Particles

M. Röthlisberger,
M. Schuck,
J. W. Kolar

Kilohertz-Frequency Rotation of Acoustically Levitated Particles

Marc Röthlisberger, Marcel Schuck and Johann W. Kolar

Abstract—The achievable rotational frequency of acoustically levitated particles is limited by the suspension stability and the achievable driving torque. In this work, a spherical ring arrangement of piezoelectric transducers and an improved excitation concept are presented to increase the rotational speed of an acoustically levitated particle by more than a factor of 10 compared to previously published results. A maximum rotational frequency of $3.6\,\mathrm{kHz}$ using asymmetric expanded polystyrene particles is demonstrated. At such rotational speeds, high frequency resonances of the transducers cause disturbances of the acoustic field which present a previously unexplored limit to the achievable manipulation rate of the particle. This limit is investigated in this work by means of calculations based on an analytical model and high precision measurements of the transducer characteristics beyond the conventional frequency range.

Index Terms—Acoustic levitation, Ultrasonics, Ultrasonic motor.

I. INTRODUCTION

TRAPPING of objects by means of acoustic forces is used in various areas such as chemistry [1], bioreactors [2], [3], blood analysis [4], study of organisms in microgravity [2], [5], control of nano material self-assembly [6], containerless processing [7], [8], [9], [10], and to study droplet dynamics [11], [12]. The main advantages of acoustic levitation over other methods, such as magnetic levitation [13], are its independence of the material properties of the object and its passive stability.

Several different arrangements of air-coupled arrays of ultrasonic transducers for levitating particles in the acoustic far field, such as single axis levitators [14], flat arrays, hemispheres, v-shaped arrays, spherical caps, and open spherical sectors [15], have been presented in the literature.

It has been demonstrated that acoustic forces can be used to rotate acoustically levitated objects. Acoustic twin traps, that require an asymmetry of the levitated object around the rotational axis to exert a torque, were used for rotational speeds up to $210\,\mathrm{rpm}$ ($f_r = 3.5\,\mathrm{Hz}$) [15], [16]. In [15], the refresh rate of the drive electronics and emitting devices was identified as the limiting factor for the manipulation rate and, therefore, the rotational speed. Acoustic vortex traps that transfer a spin angular momentum have been used for rotational speeds up to $15\,000\,\mathrm{rpm}$ ($250\,\mathrm{Hz}$) [18] for particles of radius a smaller than the acoustic wavelength ($a < \lambda$), and just below $5000\,\mathrm{rpm}$ ($83\,\mathrm{Hz}$) for particles with dimensions

M. Röthlisberger, M. Schuck and J. W. Kolar were with the Power Electronic Systems Laboratory, ETH Zürich, Switzerland (e-mail: roethlisberger@lem.ee.ethz.ch).

in the order of the acoustic wavelength [17]. In these cases, the achieved rotational speeds were limited by the levitation stability.

The acoustic pressure generated by the jth transducer of an acoustic array at a given point in space is calculated as

$$p_j = e^{i\phi}P_0 J_0(kr\sin\theta)\frac{1}{d}e^{ikd}, \tag{1}$$

where ϕ, P_0, J_0, d, θ, r and $k = \omega/c_0$ denote the phase of the transducer excitation signal, a factor depending on the electrical power ($P_0 = 0.13V_{\mathrm{ex}}$ [14]), the Bessel function of order zero, the distance of the considered point to the transducer, the beam angle, the radius of the transducer, and the wave number, respectively [15].

The pressure magnitude is proportional to the transducer excitation voltage V_{ex} [14], [19]. The overall force acting on a spherical particle with $a \ll \lambda$ in an acoustic field can be approximated by the Gor'kov potential [20].

No arrangement targeted at maximizing the levitation stability and the torque acting on an acoustically levitated particle has been presented in the literature. This work presents such an arrangement that is targeted at maximizing the achievable rotational speed of a sub-wavelength ($a < \lambda$) particle using a rotating twin trap. The required refresh rate of the drive electronics and emitting devices in the kilohertz range causes excitations of the employed ultrasonic transducers at frequencies other than their resonance frequency f_0, which imposes a previously unexplored limit in the application of such devices and on the rotational speed.

II. METHODS

A spherical ring array with a total of 80 air-coupled ultrasonic acoustic transducers, as shown in Fig. 1, was developed in this work. All transducers feature a main resonance frequency of $f_0 = 40\,\mathrm{kHz}$ and are pointed towards the center of the sphere that coincides with the levitation point of a slightly asymmetric particle. Disc-shaped expanded polystyrene (EPS) particles with a radius $a = 1\,\mathrm{mm}$ and thickness $d = 0.35 \pm 0.1\,\mathrm{mm}$ were used in this work. The goal is to maximize the acoustic pressure at this point, for which a trade-off between the total number of transducers and their distance from the levitation point exists, according to (1). The distance of all transducers to the center of the sphere is $37.5\,\mathrm{mm}$. The transducers are arranged on four vertically shifted rings, where each ring consists of 20 transducers. Four transducers each are located at the same azimuth angle, which results a favourable acoustic field distribution for high speed rotation.
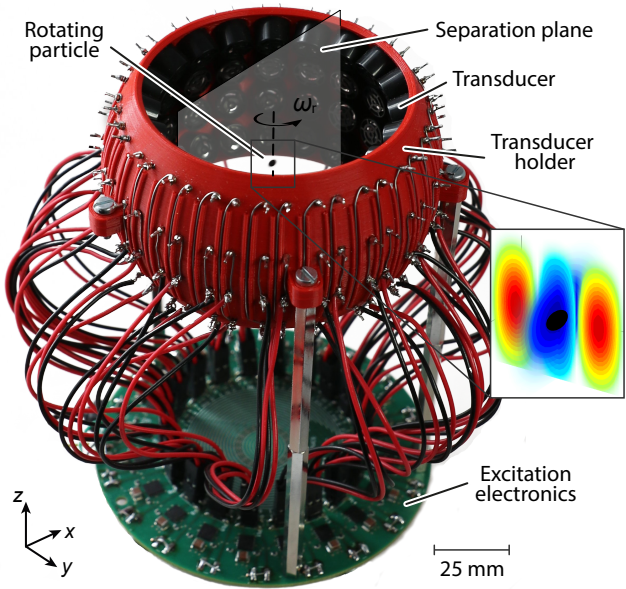
Fig. 1. Spherical ring arrangement with 80 transducers and the employed power electronics. The inset qualitatively shows the Gor'kov potential around the levitated particle.
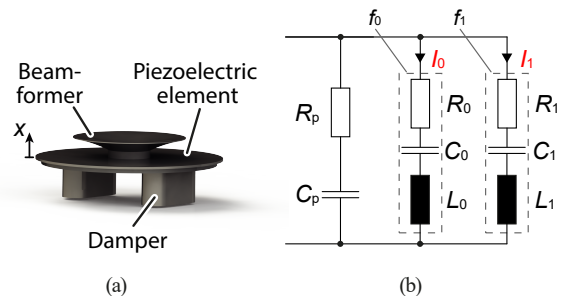

Fig. 2. Elements of the employed ultrasonic transducers (a) and Butterworth-Van-Dyke (BVD) equivalent circuit model with two resonances (b). The considered component values are listed in Table I.
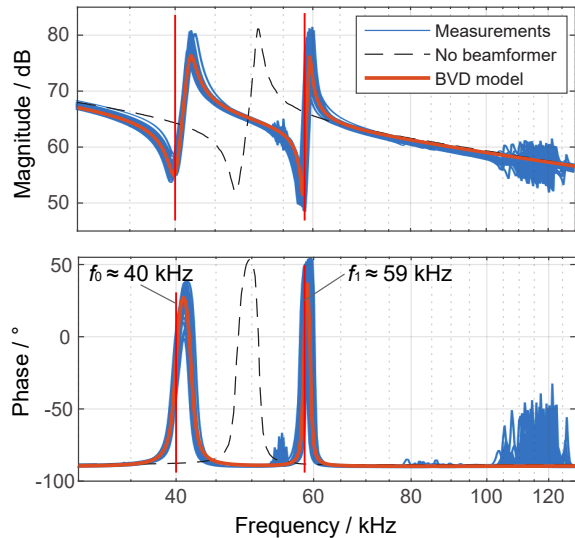

Fig. 3. Magnitude (top) and phase (bottom) of impedance measurements of 90 MSO-P1040H07T transducers compared to a fitted multi-resonance BVD model.

TABLE I
BVD MODEL PARAMETERS.

Component	Value
R_p	$5\,\Omega$
C_p	$1.75\,\mathrm{nF}$
R_0	$950\,\Omega$
C_0	$150\,\mathrm{pF}$
L_0	$103\,\mathrm{mH}$
R_1	$500\,\Omega$
C_1	$65\,\mathrm{pF}$
L_1	$113\,\mathrm{mH}$

The ultrasound transducer model MSO-P1040H07T (cf. [14]) with a diameter of $10\,\mathrm{mm}$ is used. It consists of a piezoelectric element that is mounted to a damping mass and a beamformer, as shown in Fig. 2a. The combination of the piezoelectric element and the damping mass exhibits a resonance frequency of $\approx 47\,\mathrm{kHz}$. Combined with the beamformer, the transducer has resonance frequencies at $\approx 40\,\mathrm{kHz}$ and $\approx 59\,\mathrm{kHz}$, as shown by the impedance measurements in Fig. 3. At these frequencies, a low variance in the behaviour of individual transducers can be observed, which is favourable for their application in an array. Further resonances that exhibit a large variance in their frequencies exist above $100\,\mathrm{kHz}$.

Piezoelectric transducers are commonly modelled by a Butterworth-Van-Dyke (BVD) equivalent circuit model, as shown in Fig. 2b [21], [22]. The mechanical characteristics are accounted for by the elements denoted with a subscript 0 or 1, while the elements R_p and C_p model the capacitive electrical behaviour. In most applications, ultrasonic transducers are excited at their main resonant frequency f_0 only. In this case, a single-resonance BVD model (components denoted by a subscript 0 in Fig. 2b) is sufficient to model the resulting behaviour. For achieving high rotational frequencies, excitation signals with rapidly changing phase shifts are required that cause the transducer to be excited at additional frequencies. To model the resulting mechanical behaviour of the transducer, a second resonance path, as indicated by the subscript 1 in Fig. 2b, that models the second resonance around $59\,\mathrm{kHz}$ is required.

The position of the beamformer x_m is proportional to the charge stored in the piezoelectric element and the current i_m is proportional to its velocity v_m

$$x_m - x_0 = \int_0^t v_m \mathrm{d}t = c_T \int_0^t i_m \mathrm{d}t, \qquad (2)$$

where x_0 denotes the equilibrium position of the beamformer and c_T denotes a coupling factor between the electrical model and the mechanical behaviour of the transducer.

Acoustic twin traps are used in this work as they have been found to produce high driving torques. The pressure distribution and resulting forces for such a trap generated by the spherical ring array are shown in Fig. 4. Square wave voltage signals with a fundamental frequency of $f_0 = 40\,\mathrm{kHz}$ are used to excite the transducers as they can precisely be
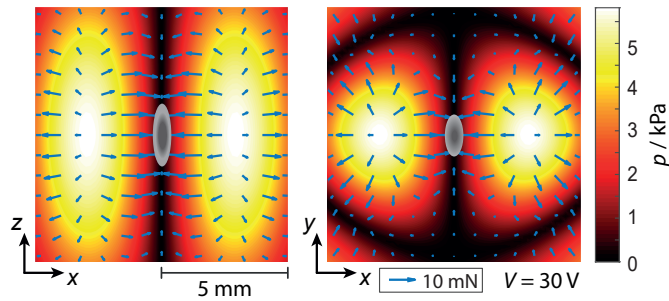
Fig. 4. Pressure distribution and forces from top view (left) and side view (right).
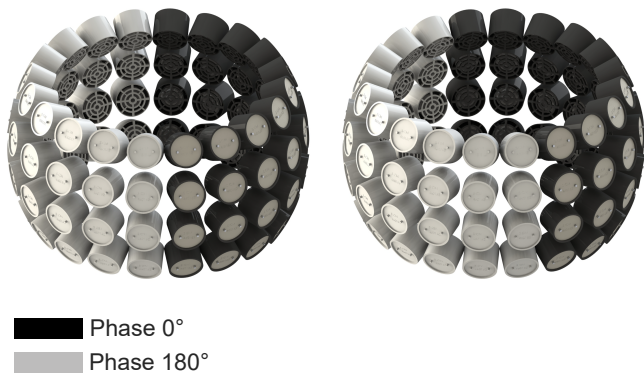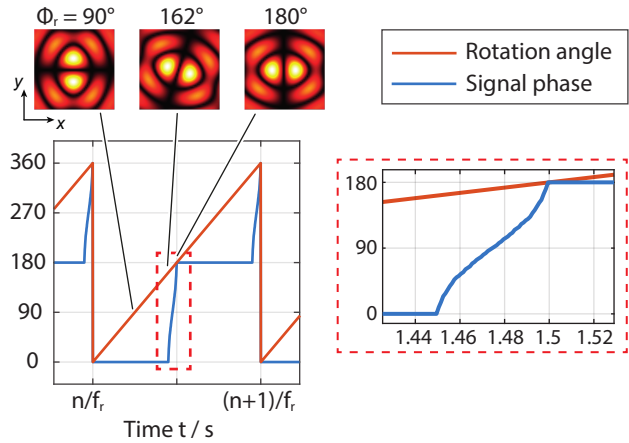

Fig. 6. Rotation angle of the particle and phase shift of the employed control concept for a single transducer over one revolution. The pressure fields are visualized for rotational angles ϕ_r of $90\,^\circ$, $162\,^\circ$, and $180\,^\circ$. The color scale is the same as in Fig. 4. The step from $162\,^\circ$ to $180\,^\circ$ shows the impact of the considered single transducer on the overall pressure distribution, where $\phi_r = 162\,^\circ$ corresponds to the point before the phase of the excitation signal is increased. The inset shows a zoomed view of the nonlinear phase increase, where the x-axis labels correspond to the fraction of the considered revolution.

Fig. 5. Phase of transducers for rotating the pressure field by $18\,^\circ$.

generated by an FPGA board (Cyclone IV) and a full-bridge power electronic switching circuit. The trap is generated by phase shifting the excitation signals of the transducers on one half of the ring by $180\,^\circ$ compared to those placed on the other half, as indicated by the plane in Fig. 1 and the color separation in Fig. 5. A rotation of the particle is achieved by rotating the acoustic field. With the proposed arrangement, the latter can be rotated by 20 discrete steps with an angular resolution of $18\,^\circ$. The phase of the transducers for one of those steps is shown in Fig. 5.

To rotate the acoustic field, as exemplary shown for three angles in Fig. 6, the phase ϕ of the excitation signal of each transducer has to be transitioned from $0\,^\circ$ to $180\,^\circ$ and from $180\,^\circ$ to $360\,^\circ$ once per revolution of the particle. To rotate the pressure field by an angle $< 18\,^\circ$, the aforementioned transition has to be carried out in multiple steps. This is required for a smooth rotation. A nonlinear gradual increase of the phase, as shown in the inset of Fig. 6, resulting in a constant rotational speed over one revolution is used. The relation between the phase and the rotation angle was found by calculating the acoustic pressure field using an analytical model based on (1). The number of excitation periods per revolution is $N = f_0/f_r$. One tenth of these periods are used for implementing the phase transitions. For increasing rotational speeds (decreasing N), the interval during which a transducer experiences a phase shift of $180\,^\circ$ becomes shorter and additional harmonics are introduced in the excitation signal, resulting in an increased deviation from the desired $40\,\text{kHz}$ signal. Particular rotational frequencies exist for which

the second resonance of the transducers is excited, resulting in an undesired disturbance of the acoustic field that prevents stable levitation. The capacitive electric behaviour of the transducer yields a decreased impedance at high frequencies, resulting in undesired current harmonics around $120\,\text{kHz}$ for high rotational speeds.

The oscillation magnitude of the transducer decreases for increasing rotational frequencies due to the inertia of its moving parts and the decreased amount of time available for the transducer to oscillate with a constant phase before the next phase change is required to rotate the particle. For a given excitation voltage, this decreases the acoustic pressure, the trapping forces, the torque, and the achievable rotational frequency. In order to quantify this effect, we measured the position of the beamformer with a Keyence LK-G5001PV Laser Displacement Sensor for different rotational speeds.

Windage losses result in a drag torque acting on the rotating particle that needs to be counteracted by the driving torque. To model the drag torque, pressure fluctuations due to the acoustic field are neglected in a first approximation. If the rotating particle is approximated by a sphere, the Reynolds number (Re)

$$\text{Re} = \frac{\rho a^2 \omega_r}{\mu}, \tag{3}$$

where ρ and μ denote the density of the surrounding fluid (air) and its dynamic viscosity, respectively, is found to be < 6000 for the considered rotational speeds in the kHz range. This corresponds to a laminar boundary layer around the particle that governs the drag torque generation, while a turbulent flow occurs further away. A model for the drag torque under these flow conditions is provided, e.g., in [23] as

$$T_{\text{drag}} = 186(\rho\mu)^{\frac{1}{2}} a^4 \omega_r^{\frac{3}{2}}. \tag{4}$$

Assuming the air in the spherical volume V_{sphere}, through which the disc rotates, is rotating at the same rotational

velocity as the disc, the drag resulting from the two sides of the disc can be neglected and the total drag is reduced compared to (4) due to the decreased disc surface $A_{\text{disc}} = 2\pi ad$ compared to the spherical surface $A_{\text{sphere}} = 4\pi a^2$, where d denotes the thickness of the disc, resulting in

$$T_{\text{drag}} = 186 \frac{A_{\text{disc}}}{A_{\text{sphere}}} (\rho\mu)^{\frac{1}{2}} a^4 \omega_{\text{r}}^{\frac{3}{2}} \tag{5}$$

for a disc shaped object, assuming the air outside of V_{sphere} stands still.

According to [24], the torque on an acoustically levitated object can be calculated as

$$T_{\text{drv}} = \int_{S_0} \mathbf{r_{CF}} \times \left(\frac{\rho}{2} \langle V^2 \rangle \mathbf{n} - \frac{1}{2\rho c^2} \langle P^2 \rangle \mathbf{n} - \rho (\mathbf{n} \cdot \mathbf{V}) \mathbf{V} \right) d\mathbf{S}, \tag{6}$$

where S_0, $\mathbf{r_{CF}}$, V, P, and $\mathbf{n}$ denote the surface of the particle, the radius from the centroid of the particle to the point of force application, the particle velocity, the pressure and the normal to the particle surface, respectively.

The drive torque for $\omega_{\text{r}} = 0$ was derived by measuring the oscillation frequency ω_{osc} after an angular step of $\Delta\alpha = 30°$ using a $1000\,\text{fps}$ camera (Sony RX 100 IV) and the OpenCV Python library for image processing. Slow motion video footage of the angle measurement is provided in the supplemental material. The measurement for an excitation voltage of $V_{\text{ex}} = 7\,\text{V}$ is shown in Fig. 7b.

The torsional spring constant K_{T} of a disc shaped object with radius a and thickness d is calculated as

$$K_{\text{T}} = \omega_{\text{osc}}^2 \frac{m}{12} (3a^2 + d^2) \tag{7}$$

The drive torque depends strongly on the angle between the disc shaped object and the symmetry plane of the twin trap. Hereinafter, this angle is referred to as the lag angle α. During rotation, the lag angle automatically adjusts, such that the driving torque equals the drag torque. For the maximum rotational speed α reaches the angle α_{max}, where the maximum driving torque is provided. This angle was determined experimentally to be $\alpha_{\text{max}} \approx 30°$. Since the torsional spring stiffness measurements were taken for a step with $\Delta\alpha = \alpha_{\text{max}}$, the driving torque can be approximated by $T_{\text{drv}} = \alpha K_{\text{T}}$ for $\alpha < \alpha_{\text{max}}$. This method is based on the one published in [24].

A stroboscope (RT Strobe Pocket LED) was used for the verification of the rotational speed. By illuminating the particle with the same frequency as the rotation frequency f_{r}, the particle appears to stand still. Due to the symmetry of the particle, it would appear to stand still for an illumination frequency of $f_{\text{i}} = 2f_{\text{r}}$ as well. To ensure that the particle rotates at f_{i} and not $\frac{f_{\text{i}}}{2}$, an additional measurement with $f_{\text{i},2} = f_r - 1\,\text{Hz}$ was carried out. For $f_{\text{r}} = f_{\text{i}}$, the particle then appears to rotate at $1\,\text{Hz}$, whereas for $f_{\text{r}} = \frac{f_{\text{i}}}{2}$, the particle would appear to rotate at $0.5\,\text{Hz}$. A video demonstrating the measurement method is provided in the supplemental material.

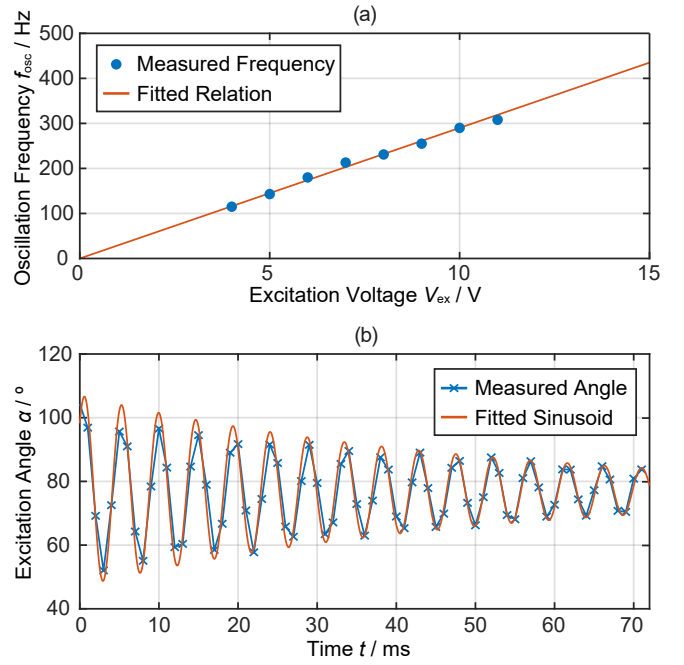Fig. 7.   Relation between the excitation voltage V_{ex} and the oscillation frequency f_{osc} measured after an angular step of $30°$ (a) and the measurement of the excitation angle α for an excitation voltage of $7\,\text{V}$ (b). The video footage used for the excitation angle evaluation is provided in the supplemental material.

III. RESULTS

The measurements of the torsional spring stiffness for different excitation voltages yielded a proportional relation between V_{ex} and the oscillation frequency ω_{osc}

$$\omega_{\text{osc}} = c_{\text{r}} V_{\text{ex}}, \tag{8}$$

where $c_{\text{r}} \approx 185.4\,\text{rad}/(\text{Vs})$ as shown in Fig. 7. According to (7), this results in a voltage dependent stand still driving torque of

$$T_{\text{drv},0}(V_{\text{ex}}) = \alpha_{\text{max}} c_{\text{r}}^2 V_{\text{ex}}^2 \frac{m}{12} (3a^2 + d^2) \tag{9}$$

yielding a driving torque of $2.6\,\mu\text{Nm}$ for the maximum excitation voltage amplitude of $37\,\text{V}$. This would result in a maximum rotational speed of about $10.3\,\text{kHz}$ according to (5) and assuming $T_{\text{drag}} = T_{\text{drv}}$.

According to the BVD model, the transducers are not capable of switching the phase instantly and the pressure and particle velocity amplitude is reduced during the transition period. This is explained by the mechanical inertia of the piezoelectric element and the beamformer. For high rotational speeds, the transition period lasts for a significant fraction of the total period between two phase shifts and the total acoustic pressure is reduced. The beamformer position for standstill and $f_{\text{r}} = 4\,\text{kHz}$ calculated using the BVD model are shown in Fig. 8. For $4\,\text{kHz}$, the excitation of the transducer is reduced approximately five times. Measurements of the beamformer position have confirmed the results obtained from the BVD model as shown in Fig. 9. For high rotational speeds, the measurements deviate slightly from the model due to small
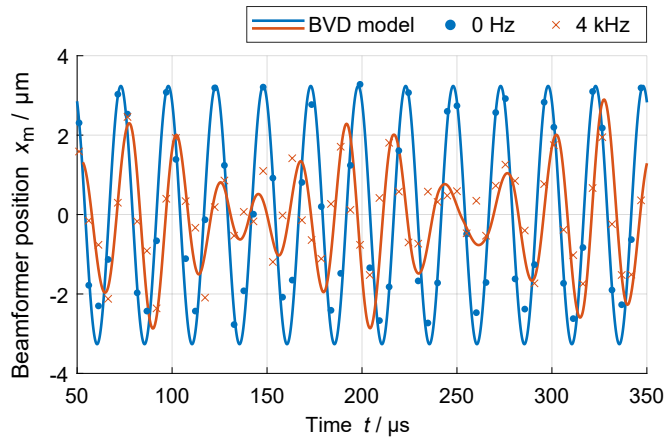
Fig. 8. Beamformer positions over time at standstill (0 rpm) and for a rotational speed of 4 kHz (240 krpm) at an excitation voltage of 30 V. The solid lines were obtained from calculations using the BVD model, the markers correspond to measured values.
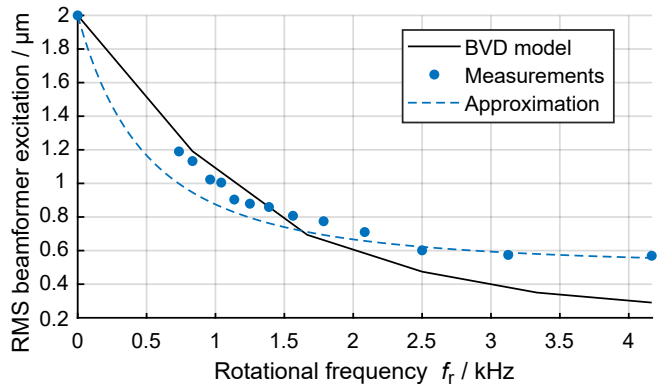

Fig. 9. RMS excitation magnitude of the beamformer for various rotational speeds at an excitation voltage of 30 V. The solid line was obtained from calculations using the BVD model, the markers correspond to measured values.

differences during the transition period. The reduced excitation of the transducers is approximated as

$$E(f_r) = \frac{3}{4\left(\frac{f_r}{1000} + 1\right)^2} + \frac{1}{4}, \qquad (10)$$

as shown in Fig. 9. As the driving torque is proportional to the pressure and particle velocity squared (cf. (6)), the driving torque is reduced by

$$T_{drv}(f_r, V_{ex}) = E(f_r)^2 T_{drv,0}(V_{ex}), \qquad (11)$$

where $T_{drv,0}(V_{ex})$ and V_{ex} denote the torque at standstill and the excitation voltage, respectively. This decreases the achievable rotational speed for an excitation voltage amplitude of 37 V from 10.3 kHz to 3.2 kHz. The drag torque T_{drag}, driving torque $T_{drv}(f_r, V_{ex})$ and measured maximum rotational speed for excitation voltage amplitudes between 8.3 and 37 V are shown in Fig. 10. For the calculation of T_{drag}, the air around the disc is assumed to stand still. Due to the rotation of the object, the air around the disc starts to move, which reduces the drag torque. This explains the difference between the drive torque required for the measured rotational speeds and the calculated drag torque shown in Fig. 10.

Based on the measurements of the beamformer position, the coupling factor between the charge stored in the transducer and the beamformer position was determined as $c_T = 76.568$ m/As (cf. (2)) for the employed MSO-P1040H07T transducers.

The disturbances for rotational speeds where large currents are flowing through resonance paths other than the one at 40 kHz were assessed by analysing the spectrum of the measured beamformer position for rotational frequencies of 500 Hz and 4 kHz. The resulting spectra are shown in Fig. 11. For 500 Hz it can be observed that oscillations occur predominantly in the desired region around 40 kHz. However, for $f_r = 4$ kHz, additional oscillations occur at the second harmonic around 60 kHz, as well as around 120 kHz. The latter constitutes a parasitic oscillation with a magnitude that
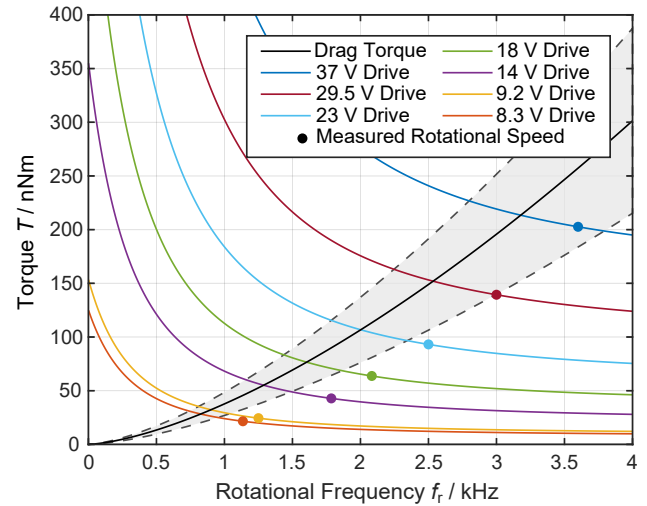

Fig. 10. Drag torque, driving torque and measured maximum rotational speed for excitation voltage amplitudes between 8.3 and 37 V. The gray area shows the error area resulting from the uncertainty of the disc thickracy, which is between $d = 0.25$ mm and $d = 0.45$ mm
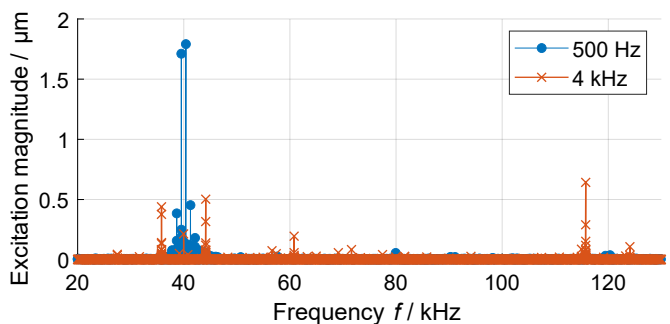

Fig. 11. Measured spectrum of the beamformer position for rotational frequencies of 500 Hz and 4 kHz.

exceeds that at lower frequencies and results in unstable levitation. The corresponding current components generate undesired losses and cause heating of the transducers. The excitation of harmonics could be reduced by using sinusoidal signals. However, such signals are more difficult to generate with switching electronic circuits.

IV. Discussion

We have demonstrated a maximum rotational speed of an acoustically levitated disc-shaped EPS particle of $216\,000\,\mathrm{rpm}$ ($f_\mathrm{r} = 3.6\,\mathrm{kHz}$). This exceeds the highest previously published value [18] by a factor of more than 14 and constitutes the highest rotational speed achieved by an acoustic levitation system to date.

We have shown that the achievable rotational speed is limited by the decreasing oscillation magnitude due to the narrow-band characteristics of the employed piezoelectric transducers and rapid changes of the phase shift of its excitation signals. This limit has not been explored previously but is relevant for other applications, where a temporal superposition of multiple pressure fields is used, such as in [17] for the levitation of objects larger than the acoustic wavelength, in [24] for the stabilization of asymmetric objects trapped in standing acoustic waves, in [25] for acoustophoretic volumetric displays and for ultrasonic haptic devices [26].

Furthermore, we have developed a new control method based on non-linear phase interpolation in order to achieve constant rotational speed.

For rapidly changing phases of the excitation signals, the current and excitation components through resonance paths other than the one at $40\,\mathrm{kHz}$ (particularly second and third harmonics) need to be carefully considered. These components can become larger than the one at the fundamental frequency, resulting in unstable levitation and high parasitic losses in the transducers.

Acknowledgment

References

[1] S. Santesson and S. Nilsson, "Airborne chemistry: Acoustic levitation in chemical analysis," *Analytical and bioanalytical chemistry*, vol. 378, pp. 1704–1709, may 2004.

[2] W. J. Xie, C. D. Cao, Y. J. Lü, Z. Y. Hong, and B. Wei, "Acoustic method for levitation of small living animals," *Applied Physics Letters*, vol. 89, no. 21, p. 214102, 2006. [Online]. Available: https://doi.org/10.1063/1.2396893

[3] J. K. R. Weber, C. Benmore, S. Tumber, A. Tailor, C. Rey, L. Taylor, and S. Byrn, "Acoustic levitation: Recent developments and emerging opportunities in biomaterials research," *European biophysical journal : EBJ*, vol. 41, pp. 397–403, oct 2011.

[4] L. Puskar, R. Tuckermann, T. Frosch, J. Popp, V. Ly, D. McNaughton, and B. R. Wood, "Raman acoustic levitation spectroscopy of red blood cells and Plasmodium falciparum trophozoites," *Lab Chip*, vol. 7, no. 9, pp. 1125–1131, 2007. [Online]. Available: http://dx.doi.org/10.1039/B706997A

[5] M. Sundvik, H. J. Nieminen, A. Salmi, P. Panula, and E. Hæggström, "Effects of acoustic levitation on the development of zebrafish, Danio rerio, embryos," *Scientific Reports*, vol. 5, no. 1, p. 13596, 2015. [Online]. Available: https://doi.org/10.1038/srep13596

[6] A. M. Seddon, S. J. Richardson, K. Rastogi, T. S. Plivelic, A. M. Squires, and C. Pfrang, "Control of Nanomaterial Self-Assembly in Ultrasonically Levitated Droplets," *The Journal of Physical Chemistry Letters*, vol. 7, no. 7, pp. 1341–1345, apr 2016. [Online]. Available: https://doi.org/10.1021/acs.jpclett.6b00449

[7] M. Röthlisberger, M. Schuck, L. Kulmer, and J. Kolar, "Contactless picking of objects using an acoustic gripper," *Actuators*, vol. 10, p. 70, 03 2021.

[8] D. Foresti, G. Sambatakakis, S. Bottan, and D. Poulikakos, "Morphing Surfaces Enable Acoustophoretic Contactless Transport of Ultrahigh-Density Matter in Air," *Scientific Reports*, vol. 3, no. 1, p. 3176, 2013. [Online]. Available: https://doi.org/10.1038/srep03176

[9] P. C. Nordine, D. Merkley, J. Sickel, S. Finkelman, R. Telle, A. Kaiser, and R. Prieler, "A levitation instrument for containerless study of molten materials," *Review of Scientific Instruments*, vol. 83, no. 12, p. 125107, dec 2012. [Online]. Available: https://doi.org/10.1063/1.4770125

[10] N. Yan, Z. Y. Hong, D. Geng, and B. Wei, "A comparison of acoustic levitation with microgravity processing for containerless solidification of ternary Al–Cu–Sn alloy," *Applied Physics A*, vol. 120, apr 2015.

[11] K. Ohsaka and E. Trinh, "Three-Lobed Shape Bifurcation of Rotating Liquid Drops," *Physical review letters*, vol. 84, pp. 1700–1703, mar 2000.

[12] C. Shen, W. Xie, and B. Wei, "Parametrically excited sectorial oscillation of liquid drops floating in ultrasound," *Physical review. E, Statistical, nonlinear, and soft matter physics*, vol. 81, p. 46305, apr 2010.

[13] H. Bleuler, M. Cole, P. Keogh, R. Larsonneur, E. Maslen, Y. Okada, G. Schweitzer, A. Traxler *et al.*, *Magnetic Bearings: Theory, Design, and Application to Rotating Machinery*. Springer, 2009.

[14] A. Marzo, A. Barnes, and B. W. Drinkwater, "TinyLev: A multi-emitter single-axis acoustic levitator," *Review of Scientific Instruments*, vol. 88, no. 8, 2017. [Online]. Available: http://dx.doi.org/10.1063/1.4989995

[15] A. Marzo, S. A. Seah, B. W. Drinkwater, D. R. Sahoo, B. Long, and S. Subramanian, "Holographic acoustic elements for manipulation of levitated objects," *Nature Communications*, vol. 6, no. May, pp. 1–7, 2015.

[16] D. Foresti and D. Poulikakos, "Acoustophoretic Contactless Elevation, Orbital Transport and Spinning of Matter in Air," *Physical Review Letters*, vol. 112, no. 2, p. 24301, jan 2014. [Online]. Available: https://link.aps.org/doi/10.1103/PhysRevLett.112.024301

[17] A. Marzo, M. Caleap, and B. W. Drinkwater, "Acoustic Virtual Vortices with Tunable Orbital Angular Momentum for Trapping of Mie Particles," *Physical Review Letters*, vol. 120, no. 4, p. 044301, jan 2018. [Online]. Available: https://link.aps.org/doi/10.1103/PhysRevLett.120.044301

[18] Z. Hong, J. Yin, W. Zhai, N. Yan, W. Wang, J. Zhang, and B. W. Drinkwater, "Dynamics of levitated objects in acoustic vortex fields," *Scientific reports*, vol. 7, no. 1, pp. 1–7, 2017.

[19] P. Fabijanski and R. Lagoda, "Modeling and identification of parameters the piezoelectric transducers in ultrasonic systems," *Advances in Ceramics-Electric and Magnetic Ceramics, Bioceramics, Ceramics and Environment*, pp. 155–176, 2011.

[20] L. P. Gor'kov, "On the Forces Acting on a Small Particle in an Acoustical Field in an Ideal Fluid," *Soviet Physics Doklady*, vol. 6, p. 773, Mar. 1962.

[21] V. T. Rathod, "A review of electric impedance matching techniques for piezoelectric sensors, actuators and transducers," *Electronics*, vol. 8, no. 2, p. 169, 2019.

[22] H. Huang and D. Paramo, "Broadband electrical impedance matching for piezoelectric ultrasound transducers," *IEEE transactions on ultrasonics, ferroelectrics, and frequency control*, vol. 58, no. 12, pp. 2699–2707, 2011.

[23] F. P. Bowden and R. G. Lord, "The aerodynamic resistance to a sphere rotating at high speed," *Proceedings of the Royal Society of London. Series A. Mathematical and Physical Sciences*, vol. 271, no. 1345, pp. 143–153, 1963. [Online]. Available: https://royalsocietypublishing.org/doi/abs/10.1098/rspa.1963.0010

[24] L. Cox, A. Croxford, B. W. Drinkwater, and A. Marzo, "Acoustic lock: Position and orientation trapping of non-spherical sub-wavelength particles in mid-air using a single-axis acoustic levitator," *Applied Physics Letters*, vol. 113, no. 5, p. 054101, 2018.

[25] T. Fushimi, A. Marzo, B. W. Drinkwater, and T. L. Hill, "Acoustophoretic volumetric displays using a fast-moving levitated particle," *Applied Physics Letters*, 2019.

[26] T. Carter, S. A. Seah, B. Long, B. Drinkwater, and S. Subramanian, "Ultrahaptics: Multi-point mid-air haptic feedback for touch surfaces," in *Proceedings of the 26th Annual ACM Symposium on User Interface Software and Technology*, 2013.